Vibrational properties of Ge nanocrystals determined by EXAFS

L. L. Araujo* and P. Kluth
Department of Electronic Materials Engineering, Research School of Physical Sciences and Engineering, Australian National University, Canberra, Australia

G. de M. Azevedo
Laboratório Nacional de Luz Síncrotron, Campinas, Brazil

M. C. Ridgway
Department of Electronic Materials Engineering, Research School of Physical Sciences and Engineering, Australian National University, Canberra, Australia

(Received 20 April 2006; revised manuscript received 9 August 2006; published 1 November 2006)

Extended x-ray absorption fine structure (EXAFS) spectroscopy was applied to probe the vibrational properties of bulk crystalline Ge (*c*-Ge) and Ge nanocrystals (Ge NCs) of 4.4 nm mean diameter produced by ion implantation in SiO_2 followed by thermal annealing. EXAFS measurements around the Ge *K* edge were carried out in the temperature range from 8 to 300 K at beam line 10-2 of the Stanford Synchrotron Radiation Laboratory (SSRL). Original information about thermal and static disorder, thermal expansion, and anharmonicity effects have been obtained for *c*-Ge and Ge NCs from temperature dependent EXAFS measurements using a correlated anharmonic Einstein model and thermodynamic perturbation theory. It was observed that the Ge NCs were stiffer (showed a stronger bond force constant) than both amorphous Ge (*a*-Ge) and *c*-Ge. Also, the values of the linear thermal expansion (thermal evolution of the mean interatomic distance) obtained for the Ge NCs were smaller than the ones obtained for *c*-Ge. These results were compared to the ones obtained for other nanocrystalline systems. They suggest that the increased surface to volume ratio of the nanocrystalline form and the presence of the surrounding SiO_2 matrix might be responsible for the different vibrational properties of *c*-Ge and Ge NCs.

DOI: 10.1103/PhysRevB.74.184102 PACS number(s): 62.25.+g, 65.80.+n, 61.46.Hk, 61.10.Ht

I. INTRODUCTION

Nanocrystalline particles are interesting subjects for materials science since their properties can deviate from those of bulk materials, making them attractive for a variety of potential applications. For example, semiconductor nanocrystals in a dielectric medium have attracted attention due to their unique optical properties which are not observed in their bulk counterparts.[1] Given that the optical properties are governed by the structural properties, characterization of the latter for Ge nanocrystals (Ge NCs) has recently been performed with the EXAFS technique[2] to attain a better understanding of the behavior of such particles. The study of Ge nanocrystals is further developed in this contribution, where EXAFS was applied to determine the short-range order vibrational properties of Ge nanocrystals synthetized in SiO_2 by ion implantation and thermal annealing.

The use of EXAFS as a vibrational probe was first suggested in the seventies[3,4] and has been explored in several ways by many research groups since that time.[5–7] Information about thermal and static disorder, thermal expansion and anharmonicity effects have been obtained for several material systems from temperature dependent EXAFS measurements. In particular, the analysis of temperature dependent data through the cumulant expansion method[8] for moderately disordered systems has proven to yield reliable information about the distribution of interatomic distances probed by EXAFS and its evolution with temperature.[5,6,9] The first three cumulants measure the average value, the variance, and the asymmetry of the distance distribution for a given coordination shell, and their variation with temperature can yield information on the linear thermal expansion, thermal disorder, and potential anharmonicity, respectively. The second and third cumulants can be related to the force constants of a one-dimensional effective pair potential from which the vibrational frequency or bond strength of the atoms in that shell can be estimated, as well as the thermal variation of the potential asymmetry. For more disordered systems it is also important to take into account the fourth term in the cumulant expansion series, called the fourth cumulant. This term accounts for symmetric deviations from a Gaussian form in the distribution of interatomic distances. The direct extraction of the thermal expansion from EXAFS data, however, is not straightforward. Care must be taken to consider effects such as the spherical nature of the photoelectron wave, the mean free path of the photoelectron and an effect that can be explained as due to the influence of vibrations perpendicular to the bond direction, as defined in Refs. 6, 9, and 10. Due to the latter, the variation of the first cumulant measured by EXAFS is different from the one calculated only from the asymmetry of the one-dimensional effective pair potential. This effect can be isolated by combining EXAFS and XRD (x-ray diffraction) results for the same system.[6,9]

Bulk crystalline Ge (*c*-Ge) has been thoroughly studied by EXAFS and other techniques (such as XRD).[2,11–13] Regarding temperature dependent EXAFS experiments, Dalba *et al.*.[6,14,15] performed systematic measurements for *c*-Ge and amorphous Ge (*a*-Ge) at temperatures from 10 to 600 K. Data were analyzed by the ratio method and results for the

first four cumulants of the distance distribution were obtained. Relative values of the cumulants were first determined (comparing low and high temperature data) and then absolute values were calculated from the relative values by fitting the high temperature data using the perturbative quantum approach of Frenkel and Rehr.[16] Low temperature quantum effects in the third cumulant and the ratio between the perpendicular and radial correlation terms were evaluated for the first shell of *c*-Ge.[6]

Moreover, Filipponi and Di Cicco performed temperature dependent EXAFS experiments for *c*-Ge at temperatures from 77 to 1100 K.[7] Data were analyzed using the GNXAS (Ref. 13) approach instead of using the cumulant expansion method and absolute values for the bond lengths and Debye-Waller factors were obtained. Other EXAFS studies of the Ge thermal expansion can be found cited within Refs. 6, 7, 14, 15, and 17.

In this work we will present results for *c*-Ge obtained by fitting experimental data with the theoretical standards given by the FEFF8.102 code,[18] which allows us to directly obtain values for the interatomic distance distributions, their variance and their asymmetry. Such values are absolute under the condition that the FEFF standard well reproduces flawless *c*-Ge. We will show that a very good agreement is found between our *c*-Ge results and those from the ratio method analysis for the first three cumulants of the first shell distance distribution. This reinforces the validity of our approach, which will then be extended to the more complex system of Ge nanocrystals embedded in a SiO_2 matrix. The study of nanoparticle systems is complicated by the superposition of surface and bulk behavior, and an EXAFS thermal expansion study should be, in principle, affected by the differences between the vibrational properties of atoms on the surface and in the core of the nanoparticles. Our comparison of bulk and nanocrystalline data should highlight the influences of size effects and the surrounding matrix on the nanocrystal vibrational properties.

There are very few temperature dependent EXAFS studies for semiconductor nanoparticle systems reported in the literature. Results obtained for Mercaptoethanol-coated ZnS nanoparticles of diameter 3.4 nm (Ref. 19) indicate that they are strained and stiffer than bulk ZnS, presenting a higher Einstein temperature. Thiol-capped CdS nanoparticles from 1.3 to 4.0 nm were also observed to show higher Einstein temperatures than bulk CdS, although the difference was higher than 5% only for the smaller nanoparticles.[20] The stiffening of the CdS bonds in the nanoparticles was assigned to their increased surface-to-volume ratio. The same effect was also observed for Thiol-capped CdTe nanocrystals.[21]

In this contribution we will present original results for the short-range order vibrational properties of an elemental semiconductor in a nanocrystalline state. The differences observed for such properties of the Ge NCs relative to the ones from bulk *c*-Ge reveal further differences between both states and allow us to get a deeper insight about size effects and the influence of a surrounding matrix of SiO_2 on the Ge NCs.

II. EXPERIMENTAL

Ge nanocrystals were formed in a 2 μm thick SiO_2 matrix by ion implantation, at liquid nitrogen temperature, of 1 $\times 10^{17}$ Ge/cm^2 at 2 MeV. The implantation was followed by thermal annealing for 1 h of the samples at 1100 °C under forming gas (95% N_2+5% H_2) flow. Further details are described in Ref. 2. The Ge peak concentration of 3 at. % was verified to be centered at a depth of 1.2 μm inside the SiO_2 layer by RBS (Rutherford backscattering spectrometry) and TEM (transmission electron microscopy) measurements.

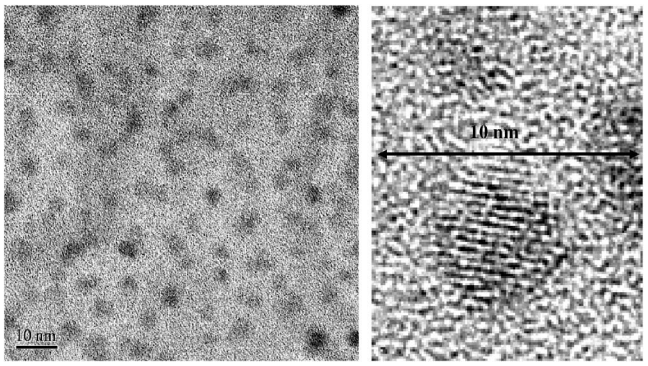

FIG. 1. XTEM images of the Ge NCs grown in SiO_2. The left frame shows the Ge NCs distributed inside the SiO_2 matrix and the right frame shows a high resolution image of one Ge NC.

Polycrystalline Ge standards of thickness 200 nm sandwiched between 2 μm thick SiO_2 layers were also produced as described in Ref. 2, for direct comparison with the nanocrystalline samples. This way, the fluorescence EXAFS measurements were carried out in similar conditions for both *c*-Ge and Ge NCs samples.

Cross section transmission electron microscopy (XTEM) results show that the nanocrystals are spherical in shape and present crystallinity similar to bulk *c*-Ge. Figure 1 presents two XTEM images of the Ge NCs as grown into the SiO_2 layer; Fig. 1(a) shows the nanocrystal distribution inside the SiO_2 layer and Fig. 1(b) shows a high resolution image of one Ge NC. Small angle x-ray scattering (SAXS) measurements (not shown here) were employed to determine the size distribution of Ge NCs. It was observed to have a mean value of 4.4 nm with a full width at half maximum of 1.5 nm.

EXAFS measurements at the Ge *K* edge (11.103 keV) were performed at temperatures from 8 to 300 K, at beam line 10-2 of the Stanford Synchrotron Radiation Laboratory, USA. Fluorescence spectra were recorded with a 30 element solid-state Ge detector and the Si (220) monochromator detuned by 50% for harmonic rejection.

The raw EXAFS data were analyzed according to the standard procedure described in Ref. 22, followed by a multiple data set fit, as will be explained below. EXAFS spectra were energy calibrated, aligned, and isolated from raw absorbance by background subtraction via the AUTOBK algorithm, as implemented in the code ATHENA.[23] Structural parameters were then determined using ARTEMIS (Ref. 23) with photoelectron momentum *k* and nonphase-corrected radial distance *r* ranges of 4.8–14.8 Å^{-1} and 1.7–2.6 Å, respectively. ATHENA and ARTEMIS are GUIs (graphical user interfaces) for the IFEFFIT code. Phases and amplitudes were calculated *ab initio* with the FEFF8.102 code.[18] The amplitude reduction factor S_0^2 and threshold energy E_0 were

determined from the polycrystalline standard and held constant thereafter at the values of 0.988 and 9.68, respectively. These are the mean values for the given temperature range, calculated from the individual values for each temperature. The coordination number was kept constant at the bulk value of 4.0 during the *c*-Ge analysis and determined for the Ge NCs as 3.2 from the lowest temperature NC spectrum. It is expected to be smaller for the nanocrystalline phase due to lower-coordinated atoms at the surface. A given data set was fitted simultaneously with multiple k weightings of 1–4, in order to reduce correlations between the fitting parameters.

III. THEORY AND DATA ANALYSIS

The information extracted from experimental spectra will be written as a series of cumulants of the distance distribution[8] for the first shell of Ge. The analysis of EXAFS data via the cumulant expansion method, as well as the relationship between the cumulants and the local dynamics in crystalline materials, has recently been reviewed by Fornasini *et al.*[9]

The EXAFS second cumulant, MSRD (mean square relative displacement) or Debye-Waller factor σ^2 is sensitive to both structural and thermal disorder. As the structural component is considered not to vary with temperature, it is possible to separate both contributions by performing temperature dependent EXAFS measurements and fitting the resultant Debye-Waller factors with a Debye or Einstein model.[24] For the σ^2 of the first shell of Ge, in particular, the correlated Einstein model is considered a suitable choice.[25,26] The EXAFS σ^2 can yield information on the vibrational dynamics of both crystalline and noncrystalline materials.[24] It contains effects of correlation between the atomic motion of absorber and backscatterer atoms, differing from the XRD MSD (mean square displacement) by the DCF (displacement correlation function).[3] On more general grounds, the temperature dependence of the σ^2 provides a measure of the effective bond-stretching force constant between absorber and backscatterer atoms and can be used to study the strength of chemical bonds.

The third cumulant of the distance distribution C_3 measures its asymmetry. C_3 can be different from zero even for a harmonic crystal at very low temperatures due to the effect of zero-point atomic vibrations.[9] In samples that are not flawless crystals, further asymmetry in the distribution of distances may be observed. But this static contribution is not supposed to increase with temperature, so that the variation of C_3 with temperature can be ascribed to asymmetry in the distance distribution generated by anharmonicity of the effective interaction potential.

A. Relationship between thermal expansion and EXAFS cumulants

A relationship between a linear thermal expansion factor a and the EXAFS cumulants in the quantum limit was derived by Frenkel and Rehr using a correlated anharmonic Einstein model and thermodynamic perturbation theory.[16] In this model, a one-dimensional anharmonic *effective* pair potential of the form

$$V(r-r_0) = k_e(r-r_0)^2 - k_3(r-r_0)^3 + \cdots \quad (1)$$

was assumed, where r_0 is the minimum of the effective pair potential, k_e is the effective harmonic spring constant, and k_3 is the cubic anharmonicity constant. The following relationships were then derived for the temperature dependence, to leading order in k_3, of the second cumulant σ^2, third cumulant C_3, and linear thermal expansion factor a (connected to the thermal variation of the first cumulant C_1), respectively[5,16]

$$C_2(T) = \sigma^2(T) = \frac{\hbar\omega_E}{2k_e}\frac{1+z}{1-z} + \sigma^2_{static}, \quad (2)$$

$$C_3(T) = \frac{k_3(\hbar\omega_E)^2}{2k_e^3}\frac{1+10z+z^2}{(1-z)^2} + C_{3static}, \quad (3)$$

$$a(T) = \frac{3}{2}\frac{\hbar k_3}{\mu^2\omega_E^3}\frac{1+z}{1-z}, \quad (4)$$

where T is the temperature, ω_E is the Einstein frequency ($k_e=\mu\omega_E^2$), μ is the reduced mass (in this case, for a Ge-Ge absorber-scatterer pair), and $z\equiv\exp(-\Theta_E/T)$. The Einstein temperature is given by $\Theta_E=\hbar\omega_E/k_B$, where k_B is the Boltzmann constant. σ^2_{static} and $C_{3static}$ are the static or structural (temperature independent) contributions to the total disorder and asymmetry, respectively. These terms have been added here to the temperature dependent ones in order to account for the effects of static disorder, expected to be different for *c*-Ge and Ge NCs.[2,22]

This one-dimensional model can be used as a reference to analyze the thermal behavior of the cumulants of the distance distribution obtained from experimental EXAFS data. It can be considered as the *effective* potential of the one-dimensional distribution of distances sampled by the EXAFS analysis of a given shell of a three-dimensional crystalline (or nanocrystalline) material.

B. EXAFS *effective* and *real* distance distributions

In an experimental measurement the EXAFS photoelectrons (with mean free path λ) probe an *effective* distance distribution $P(r,\lambda)=\rho(r)^*\exp(-2r/\lambda)^*r^{-2}$, due to the weakening of the photoelectron wave with distance, the spherical nature of such a wave and the finite mean free path.[8] On the other hand, the instantaneous interatomic distances r are distributed according to the *real* unidimensional distribution $\rho(r)$. For systems with low to moderate disorder, the difference between the cumulants of both distributions is considered non-negligible only for the first cumulant (interatomic distance),[6,8] and this difference must be kept in mind when a thermal expansion study is undertaken.

As the analysis of EXAFS experimental data by comparison with FEFF generated standards using the IFEFFIT code accounts for the effects of the weakening of the photoelectron wave with distance, the spherical nature of such a wave and the finite mean free path, the values obtained from such method are the *real* cumulants of the distance distribution.

Thus, they can be directly applied in a thermal expansion study.

C. Effective pair potential and distance distributions

The use of an effective pair potential to describe the distribution of distances probed by EXAFS must be applied with care in order to take into account some of its limitations. The effective pair potential can be, in principle, temperature dependent, both in position and shape.[27] In particular, a positive shift of the minimum of the effective pair potential was assigned to the effect of vibrations perpendicular to the bond direction, among other causes.[9,27] This suggests that the thermal expansion probed by EXAFS depends not only on the asymmetry of the effective potential (given by the second and third cumulants, σ^2 and C_3), as implied in Frenkel and Rehr's model, but also on its rigid shift. Stern (Ref. 10) also points out the importance of the vibrations perpendicular to the bond direction and explains the rigid shift as a consequence of the difference in the minimum of the *effective* and *real* potentials, i.e., the difference between the maximum of the *effective* and *real* distributions of interatomic distances. Furthermore, for bulk AgI and CdSe, a variation of the minimum of the effective potential with temperature has been reported,[28,29] shifting to lower values as the temperature increased; such an effect was not observed for Ge.[9]

As a result, the temperature variation of the EXAFS *real* first cumulant and the linear thermal expansion factor a as given above cannot be considered equivalent. In order to avoid misinterpretations due to differences in both quantities, here the quantity a as defined in Ref. 16 [reproduced in Eq. (4) above] will be called the anharmonic contribution to the thermal expansion, since it is related to the anharmonicity of the effective potential only. The variation of our first cumulant with temperature, δC_1, will be called the EXAFS thermal expansion and will include contributions not only due to the anharmonicity but also due to the shift of the effective potential. The difference between the EXAFS δC_1 and XRD δR thermal expansions will be connected to the shift of the effective potential (perpendicular vibrations), rather than to its asymmetry.

D. Data analysis

Theoretical spectra were simulated by the FEFF 8.102 code (Ref. 18) and the values of the cumulants of the distance distribution for the first shell of Ge were obtained through a nonlinear best fit to experimental spectra using ARTEMIS.[23,30]

The analysis of experimental spectra was carried out in two steps. In the first one, each spectrum was fitted at once, giving separate values of C_1, σ^2, C_3. The presence of a fourth cumulant C_4 was also considered in the fits, but it was observed to be negligible for all measurements. This confirmed the validity of deriving the cumulant equations from (4) to leading order in k_3.

Although the σ^2 values obtained this way were insensitive to small variations in the fitting conditions and presented small error bars, the same was not observed for the C_1 and C_3 values, due to the correlation between these quantities. A similar result was observed by Fornasini *et al.* when analyzing the EXAFS data for the thermal expansion of bulk Cu.[27] We then fitted our obtained σ^2 results as a function of temperature according to Eq. (2), obtaining the Einstein temperature (and consequently ω_E and k_e).

In the second step, the variation of the second and third cumulants σ^2 and C_3 with temperatures were restrained to follow Eqs. (2) and (3) and all spectra from 8 to 300 K were fitted simultaneously, in a similar way to the methods described in Refs. 20 and 31. Representing the evolution of the second cumulant by the correlated Einstein model and of the third cumulant by Eq. (3) is appropriate since both quantities have shown to be well described by these models in the literature. The thermal variation of the first cumulant C_1, on the other hand, was not restrained to follow Eq. (4) since it is, in principle, not well represented by its variation with the asymmetry of the potential only. Thus, the first cumulant for each temperature was simply written as r_0+dr_T, where r_0 is the value of the first cumulant for the lowest temperature data. During the multiple data set fit, k_e was fixed to the value obtained from the fit to the σ^2 from the first step, so that k_3, the structural contribution to C_3, r_0, and the dr_T for each temperature were the only fitting parameters. By doing this, the number of free parameters was reduced and the C_3 values and variation were linked to the ones of the second cumulant, helping to decrease the errors in its determination and to break the correlation between C_3 and C_1.

IV. RESULTS AND DISCUSSION

Figure 2 shows the Fourier transforms of a selection of the temperature dependant k^3-weighted EXAFS spectra as a function of the radial distance (without phase corrections) obtained in this work. Figure 2(a) shows spectra measured at 8, 100, and 300 K for c-Ge, while Fig. 2(b) shows spectra measured at the same temperatures for Ge NCs. Comparing the data for the two systems, some characteristic features of

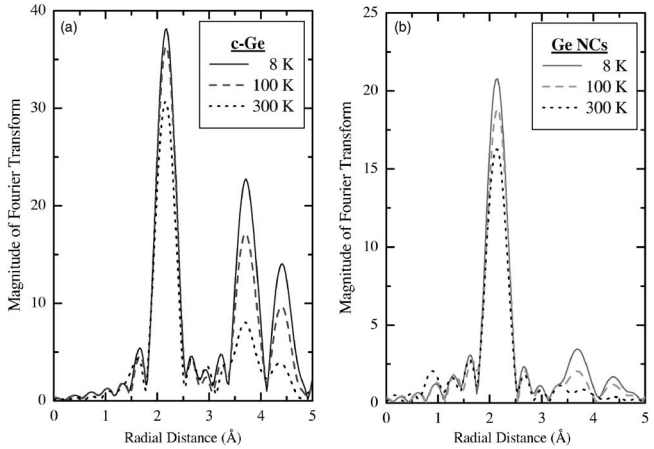

FIG. 2. Fourier transforms of k^3-weighted EXAFS spectra as a function of the nonphase-corrected radial distance measured at different temperatures for (a) polycrystalline Ge and (b) Ge nanocrystals.

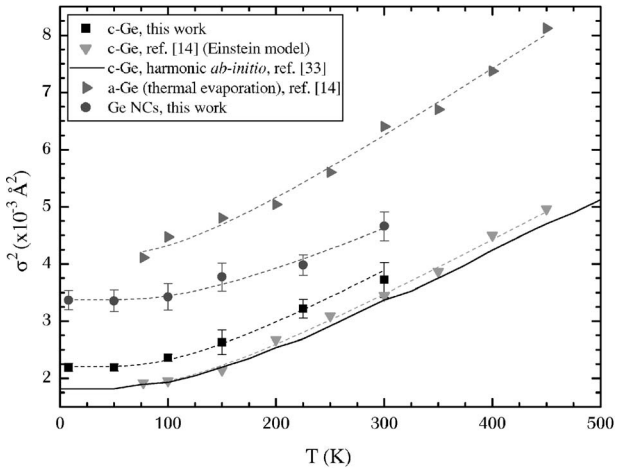

FIG. 3. Debye-Waller factor σ^2 values for several Ge systems (symbols, see figure legend) as a function of the measurement temperatures, with the respective correlated Einstein model fits (dashed lines). The solid line shows the *ab initio* harmonic calculation for the thermal contribution to σ^2 for a *c*-Ge system.

nanocrystalline materials become readily apparent. For example, at any given temperature the magnitude of the Fourier transforms is lower for the Ge NCs due to their higher surface to volume ratio, which causes a reduction of the overall coordination number and an increase in the variance of the distance distributions compared to the bulk *c*-Ge ones. Also, the second and third neighbor shells are less pronounced for the Ge NCs since they are more sensitive to variations in bond angles, which is also a result of the increased surface to volume ratio. Furthermore, the damping of the amplitude of the EXAFS signal with increasing temperature for both systems can be verified from the graphs.

A. Debye-Waller factors and Einstein temperatures

The Debye-Waller factor values obtained for both *c*-Ge and Ge NCs from our experimental spectra are shown as a function of the measurement temperatures in Fig. 3. Also plotted for comparison are the data for crystalline and amorphous Ge published previously in Ref. 14. The lines are the respective fits with the correlated Einstein model as given by Eq. (2) for each data set. The values obtained from such fits for the static contribution to the total disorder and for the thermal one (given in terms of the Einstein temperatures) are shown in Table I.

As it can be seen, our temperature dependent Debye-Waller factor data for crystalline Ge show the same temperature evolution as the data from Ref. 14, but their absolute values differ by a constant offset. This offset could correspond to a static disorder contribution, which in principle is not expected for bulk *c*-Ge. But the offset can also be the result of experiment artifacts in fluorescence EXAFS measurements. In order to evaluate such effects we have considered normalization, I_0 chamber and self-absorption corrections. They were calculated using the program TkATOMS (Ref. 32) with the Elam tables for x-ray absorption cross sections.[33] The normalization correction accounts for the energy-dependent attenuation of the amplitude of the EXAFS signal introduced by the edge-step normalization. It was estimated as 0.000 05 Å^2 in our experiments. The I_0 correction accounts for the fact that the energy dependence to I_0 is disregarded when the absorption cross section is calculated as a function of the incident and fluorescence emitted photons. The I_0 chamber used in the experiments was 15 cm long and filled with N_2, yielding a correction of 0.000 27 Å^2. Finally, the self-absorption correction accounts for the apparent amplitude reduction due to the self-absorption of the fluorescing photons by the sample before they reach the detector. This contribution is negligible for our samples as they are much thinner than one absorption length for the *K* edge of Ge.[2] The absorption length is 9.5 μm while the *c*-Ge samples are 0.2 μm thick, which amounts to 2.1% of an absorption length. The Ge NCs samples have even smaller amounts of Ge so that this contribution is even smaller for them. Adding up these corrections it becomes apparent that the offset between the crystalline Ge data corresponds to experiment induced effects rather than to static contribution to the disorder present in the sample. When this offset is subtracted from our data, an excellent agreement is found for both crystalline Ge datasets. Strauch *et al.* have used *ab initio* phonon dynamics calculations to compute Debye-Waller factors for the first three shells of *c*-Ge in the harmonic approximation.[34] Their results, which do not include static contributions to the second cumulant, are also shown in Fig. 3. We can see a non-negligible difference between the calculations and the experimental data which indicates that some anharmonicity is present even for the first shell above $T \sim 150$ K.

TABLE I. Einstein temperatures and static components of the Debye-Waller factors obtained from best fits of the correlated Einstein model to the experimental temperature dependent data.

SYSTEM	Θ_E (K)	σ^2_{static} (X10^{-3}Å^2)
c-Ge, Ref. 14	355.3±5.7	0 (set)
c-Ge, this work	351.1±7.2	0.34±0.05
Ge NCs, this work	391.4±11.2	1.70±0.07
a-Ge (sputtering), Ref. 17	344.9±3.3	1.98±0.04
a-Ge (evaporation), Ref. 14	323.3±4.7	2.13±0.10

The Debye-Waller factors for two *a*-Ge samples prepared by different techniques showed a similar trend with a slight difference in absolute values.[14,17] For clarity, only the data from Ref. 14 is plotted in Fig. 3. The sample prepared by thermal evaporation exhibited higher static disorder than the sample prepared by sputter deposition, as listed in Table I. These results were compared in Ref. 17, where the effect of hydrogenation of *a*-Ge samples (not shown here) was also discussed. We will concentrate on the fact that both samples show higher static contribution to σ^2 and lower Einstein temperatures than both the *c*-Ge and Ge NCs samples.

The static contribution to the Debye-Waller factor for Ge NCs grown by ion-implantation inside a SiO_2 matrix lies between that of *c*-Ge and *a*-Ge. This indicates that the nanocrystals are in a state of higher configurational energy than the crystalline samples, but are not in a state as disordered as

the amorphous phase. The higher static disorder in the NCs when compared to *c*-Ge originates from both the reconstruction of the NCs surface due to the presence of undercoordinated atoms and the internal strain in the crystalline core.[19]

Furthermore, the thermal evolution of the Debye-Waller factor for the nanocrystals is slower than the ones for both *c*-Ge and *a*-Ge, as can be observed by the smaller slope of the curve best fitting the data. It must be pointed out that the same corrections estimated for *c*-Ge (normalization, I_0 and self-absorption) also apply to the case of Ge NCs.

As for the Einstein temperatures, it was observed that the value best fitting the Debye-Waller factor data is higher in the *c*-Ge samples than in both *a*-Ge samples, suggesting a softening of the compression modes in the amorphous phase. On the other hand, the Einstein temperature best fitting the NC data (391 K) is higher than the *c*-Ge ones (351 and 355 K), indicating that the nanocrystals are stiffer than the bulk (have stiffer bonds). This finding is in agreement with the results obtained for ZnS nanoparticles,[19] which were reported to be strained and stiffer than the bulk ZnS. The stiffening of ZnS nanoparticles could not be explained only by the radial compression of the nanoparticles, nor by simple models such as linear strain or surface-weighted radial strain, and was assigned to inhomogeneous internal strain caused by competing relaxations at the surface. On the contrary, most metallic nanoparticles appear to behave the opposite way, showing Einstein temperatures lower than the ones observed for the bulk, as reported in Refs. 35–41. Since the binding characteristics (electronic structure) of metals and semiconductors are fundamentally different in their bulk form, it is not surprising to observe differences between them in the nanocrystalline form. While covalent bonds tend to be stiffer and very directional, metallic bonds are softer and less directional, what gives more freedom to surface atoms to move in metallic nanocrystals, hence the differences between metallic and semiconductor nanocrystals.

The harmonic spring constants k_e of the effective pair potential obtained from the Einstein temperatures of Table I amount to 8.1 eV/Å^2 for our *c*-Ge, which is in good agreement with the value obtained for *c*-Ge in Ref. 6, 8.5 eV/Å^2. The value of 10.1 eV/Å^2 obtained for our Ge NCs corresponds to the higher Einstein temperature obtained from the fits for this system.

B. Third cumulants

The results obtained in the present work for the third cumulant C_3 are shown in Fig. 4. They were obtained restraining the temperature dependent C_3 values to follow Eq. (3) during the multiple data set fits. Also, the results for *c*-Ge from Ref. 6 and *a*-Ge from Ref. 17 are plotted for comparison. The C_3 values for both crystalline samples are in very good agreement. At temperatures below 150 K they are very small, but different from zero due to low temperature quantum effects and the zero point motion.[6] From 150 K onwards, the C_3 values show a parabolic raise that is consistent with the classical approximation.

The same trend can be observed for the *a*-Ge data with a constant offset which shifts the data to higher total values, probably due to a static contribution to C_3.

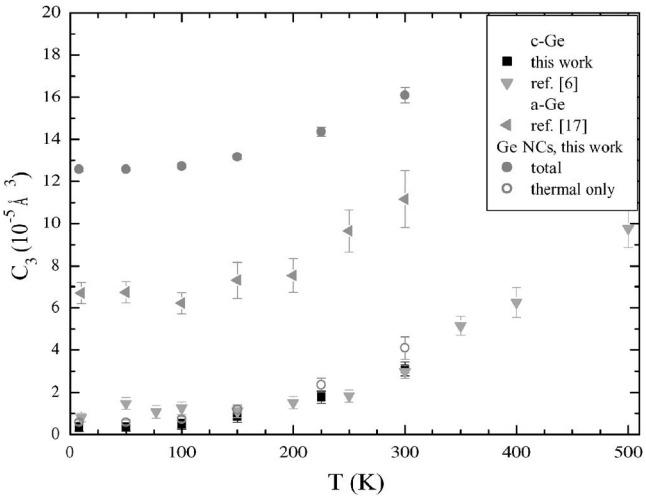

FIG. 4. Values of the third cumulant of the distance distributions C_3 for *c*-Ge, *a*-Ge, and Ge NCs. The thermal contribution to C_3 of the Ge NCs is also plotted individually for comparison.

For the Ge NCs, however, the picture is somewhat different. Even at low temperatures, the total values of C_3 are considerably higher than for *c*-Ge and *a*-Ge. This is caused by the higher asymmetry in the distribution of distances for the NCs, giving rise to a static contribution of 12×10^{-5} Å^3 to C_3 in all the temperature range. Depending on the ratio between surface and core atoms and the strain induced in the crystalline core, the asymmetry in the distribution of distances can be significant for the NCs, even at low temperatures. Thus, we ascribe this difference to static asymmetry due to the relaxation/reconstruction of the surface atoms and the internal strain existing in the Ge NCs.

The thermal only contribution to the C_3 of the NCs, also plotted in Fig. 4, evolves with temperature only at a slightly higher rate than for the crystalline sample. This indicates that the temperature induced asymmetry is of similar magnitude for the nanocrystals and bulk Ge in the temperature range under consideration.

C. First cumulants and linear thermal expansion

The mean interatomic distances obtained from the fits to the experimental spectra correspond to our first cumulant C_1, whose values are shown in Fig. 5 for *c*-Ge and Ge NCs. Their variation with temperature gives the local linear thermal expansion for the first shell. Comparing the EXAFS thermal expansion to the crystallographic or XRD thermal expansion (from Ref. 42) for *c*-Ge, we can see that their difference increases with temperature. This behavior can be assigned to the effect of perpendicular vibrations, as mentioned earlier.[6,9,10] By comparing both data, it is possible to calculate the perpendicular MSRD for *c*-Ge, as it has been done in Ref. 6.

As for the Ge NCs, the thermal increase of the mean interatomic distance was verified to evolve slower with the increase of temperature when compared to *c*-Ge. The higher value of C_1 for the Ge NCs at 8 K is assigned to structural differences between the crystalline and nanocrystalline phases.

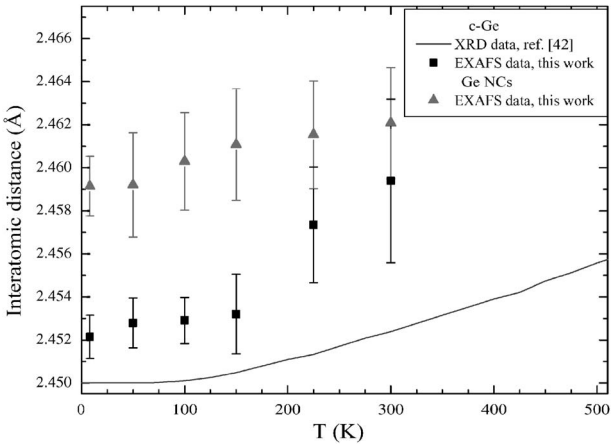

FIG. 5. Thermal evolution of the interatomic distances for *c*-Ge and Ge NCs as given by the variation of the first cumulant or mean interatomic distance, symbols. The full line is the thermal evolution of the distance between the equilibrium positions of the atoms as given by XRD.[42]

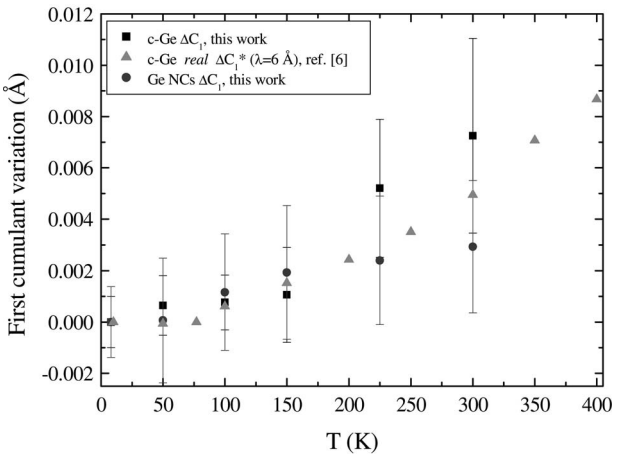

FIG. 6. Relative values of the first cumulant of the distance distribution for the first shell of Ge.

In order to compare our first cumulant C_1 obtained for *c*-Ge with the *real* first cumulant C_1^* obtained through the ratio method analysis in Ref. 6, we calculated the ΔC_1 values shown in Fig. 6, where Δ means the variation relative to the lowest temperature data, i.e., $\Delta C_1(T)=C_1(T)-C_1(8\ \mathrm{K})$. This is necessary because the ratio method provides only relative values for the *effective* first cumulant, which are taken with the lowest temperature data as the reference value. The relative values of the *real* first cumulant ΔC_1^* are then calculated from the *effective* ones, as described in Refs. 6 and 15. It can be seen that the relative values of our first cumulant ΔC_1 and the ones from the *real* first cumulant ΔC_1^* (calculated in Ref. 6 considering $\lambda=6$ Å) are in good agreement at lower temperatures, where the values are really small, but at higher temperatures there is a disagreement of about 0.002 Å. Such a disagreement might originate from the different way of treating the k dependence of the mean free path λ and of handling the conjugate variable to the distance r in both approaches. While in the ratio method analysis applied in Ref. 6 a constant value for λ was used to convert *effective* to *real* interatomic distances, here the k dependence of λ is calculated from the imaginary part of the interaction potential during the data analysis.

V. CONCLUSIONS

We have verified that the thermal properties of Ge NCs differ significantly from the ones observed for both *c*-Ge and *a*-Ge. Using our approach, we were able to reproduce the thermal behavior of the EXAFS cumulants previously obtained for the first shell of bulk *c*-Ge through the ratio method[6] and also obtain original results for Ge NCs.

Our results for Ge NCs show that they exhibit a higher Einstein temperature than both *a*-Ge and *c*-Ge, indicating stiffer bonds. It was also verified that the linear thermal expansion for Ge NCs is smaller than for *c*-Ge. These findings are in good agreement with existing data for other nanocrystalline semiconductor systems.[19–21] The fact that the thermal evolution of the first cumulant is lower for the NCs than for the bulk while the thermal evolution of the third cumulant is slightly higher strengthens the argument that the variation of the EXAFS first cumulant should not be considered as given only by the quantity a from the Frenkel-Rehr model.[16] In other words, it supports the assumption that the variation of the third cumulant should not be used to estimate the thermal expansion or variation with the temperature of the interatomic distances measured by EXAFS.

In a recent work,[43] it was shown that Ge NCs produced in SiO_2 by ion implantation are subject to a strong compressive stress in their as-grown state. This could be one of the reasons for the observed damping in the thermal expansion for Ge NCs when compared to the ones for *c*-Ge. If the interaction between the SiO_2 matrix and the Ge atoms on the surface of the nanocrystals is not negligible, the matrix may suppress the movement of such atoms, increasing their stiffness. Furthermore, the stronger this matrix-surface atoms interaction is, the higher the static disorder could be.

A new study is being carried out in order to further clarify the influence of the SiO_2 matrix over the vibrational properties of the Ge NCs.

ACKNOWLEDGMENTS

L.L.A. and G.de M.A. acknowledge the Brazilian agency CNPq (Conselho Nacional de Desenvolvimento Científico e Tecnológico) for financial support. P.K. and M.C.R. acknowledge the Australian Research Council and Australian Synchrotron Research Program for financial support. Portions of this research were carried out at the Stanford Synchrotron Radiation Laboratory, a national user facility operated by Stanford University on behalf of the U.S. Department of Energy, Office of Basic Energy Sciences.

*Corresponding author. Electronic address: lla109@rsphysse.anu.edu.au

[1] L. Rebohle, J. von Borany, H. Fröb, and W. Skorupa, Appl. Phys. B **71**, 131 (2000).
[2] M. C. Ridgway, G. de M. Azevedo, R. G. Elliman, C. J. Glover, D. J. Llewellyn, R. Miller, W. Wesch, G. J. Foran, J. Hansen, and A. Nylandsted-Larsen, Phys. Rev. B **71**, 094107 (2005).
[3] G. Beni and P. M. Platzman, Phys. Rev. B **14**, 1514 (1976).
[4] E. Sevillano, H. Meuth, and J. J. Rehr, Phys. Rev. B **20**, 4908 (1979).
[5] L. Tröger, T. Yokoyama, D. Arvanitis, T. Lederer, M. Tischer, and K. Baberschke, Phys. Rev. B **49**, 888 (1994).
[6] G. Dalba, P. Fornasini, R. Grisenti, and J. Purans, Phys. Rev. Lett. **82**, 4240 (1999).
[7] A. Filipponi and A. Di Cicco, Phys. Rev. B **51**, 12322 (1995).
[8] G. Bunker, Nucl. Instrum. Methods Phys. Res. **207**, 437 (1983).
[9] P. Fornasini, F. Monti, and A. Sanson, J. Synchrotron Radiat. **8**, 1214 (2001).
[10] E. A. Stern, J. Phys. IV **7**, C2–137 (1997).
[11] P. A. Lee, P. H. Citrin, P. Eisenberger, and B. M. Kincaid, Rev. Mod. Phys. **53**, 769 (1981).
[12] J. Mustre de Leon, J. J. Rehr, S. I. Zabinsky, and R. C. Albers, Phys. Rev. B **44**, 4146 (1991).
[13] A. Filipponi and A. Di Cicco, Phys. Rev. B **52**, 15135 (1995).
[14] G. Dalba, P. Fornasini, M. Grazioli, and F. Rocca, Phys. Rev. B **52**, 11034 (1995).
[15] G. Dalba, P. Fornasini, R. Grisenti, and J. Purans, J. Synchrotron Radiat. **6**, 253 (1999).
[16] A. I. Frenkel and J. J. Rehr, Phys. Rev. B **48**, 585 (1993).
[17] G. Dalba, P. Fornasini, R. Grisenti, F. Rocca, I. Chambouleyron, and C. F. O. Graeff, J. Phys.: Condens. Matter **9**, 5875 (1997).
[18] A. L. Ankudinov, B. Ravel, J. J. Rehr, and S. D. Conradson, Phys. Rev. B **58**, 7565 (1998).
[19] B. Gilbert, F. Huang, H. Z. Zhang, G. A. Waychunas, and J. F. Banfield, Science **305**, 5684 (2004); **305**, 651 (2004).
[20] J. Rockenberger, L. Tröger, A. Kornowski, T. Vossmeyer, A. Eychmüller, J. Feldhaus, and H. Weller, J. Phys. Chem. B **101**, 2691 (1997).
[21] J. Rockenberger, L. Tröger, A. Rogach, M. Tischer, M. Grundmann, A. Eychmüller, and H. Weller, J. Chem. Phys. **108**, 7807 (1998).
[22] M. C. Ridgway, G. de M. Azevedo, C. J. Glover, R. G. Elliman, D. J. Llewellyn, A. Cheung, B. Johannessen, D. A. Brett, and G. J. Foran, Nucl. Instrum. Methods Phys. Res. B **218**, 421 (2004).
[23] B. Ravel and M. Newville, J. Synchrotron Radiat. **12**, 537 (2005).
[24] G. Dalba and P. Fornasini, J. Synchrotron Radiat. **4**, 243 (1997).
[25] E. A. Stern, in *X-Ray Absorption: Principles, Applications, Techniques of EXAFS, SEXAFS and XANES*, edited by D. C. Koningsberger and R. Prins (Wiley, New York, 1988), p. 20.
[26] G. S. Knapp, H. K. Pan, and J. M. Tranquada, Phys. Rev. B **32**, 2006 (1985).
[27] P. Fornasini, S. a Beccara, G. Dalba, R. Grisenti, A. Sanson, M. Vaccari, and F. Rocca, Phys. Rev. B **70**, 174301 (2004).
[28] G. Dalba, P. Fornasini, R. Grisenti, D. Pasqualini, D. Diop, and F. Monti, Phys. Rev. B **58**, 4793 (1998).
[29] G. Dalba, P. Fornasini, R. Gotter, and F. Rocca, Phys. Rev. B **52**, 149 (1995).
[30] M. Newville, B. Ravel, J. Rehr, E. Stern, and Y. Yacoby, Physica B **208-209**, 154 (1995).
[31] K. A. Daly and J. E. Penner-Hahn, J. Synchrotron Radiat. **5**, 1383 (1998).
[32] B. Ravel, J. Synchrotron Radiat. **8**, 314 (2001).
[33] W. T. Elam, B. Ravel and J. R. Sieber, Radiat. Phys. Chem. **63**, 121 (2002).
[34] D. Strauch, P. Pavone, N. Nerb, K. Karch, W. Windl, G. Dalba, and P. Fornasini, Physica B **219**, 436 (1996).
[35] T. Yokoyama, S. Kimoto, and T. Ohta, Jpn. J. Appl. Phys., Part 1 **28**, L851 (1989).
[36] T. Yokoyama and T. Ohta, Jpn. J. Appl. Phys., Part 1 **29**, 2052 (1990).
[37] A. Balerna and S. Mobilio, Phys. Rev. B **34**, 2293 (1986).
[38] C. Solliard, Solid State Commun. **51**, 947 (1984).
[39] M. A. Marcus, M. P. Andrews, J. Zegenhagen, A. S. Bommannavar, and P. Montano, Phys. Rev. B **42**, 3312 (1990).
[40] E. C. Marques, D. R. Sandstrom, F. W. Lytle, and R. B. Greegor, J. Chem. Phys. **77**, 1027 (1982).
[41] M. Dubiel, S. Brunsch, and L. Tröger, J. Synchrotron Radiat. **8**, 539 (2001).
[42] Y. S. Touloukian, R. K. Kirby, R. E. Taylor, and P. D. Desay, *Thermophysical Properties of Matter* (Plenum, New York, 1977), Vol. 13.
[43] I. D. Sharp, D. O. Yi, Q. Xu, C. Y. Liao, J. W. Beeman, Z. Liliental-Weber, K. M. Yu, D. N. Zakharov, J. W. Ager III, D. C. Chrzan, and E. E. Haller, Appl. Phys. Lett. **86**, 063107 (2005).